Autonomous Fault Detection with Carrier-Phase DGPS for Shipboard Landing Navigation

MOON-BEOM HEO and BORIS PERVAN
Illinois Institute of Technology, Chicago, Illinois

SAM PULLEN, JENNIFER GAUTIER, and PER ENGE
Stanford University, Stanford, California

DEMOZ GEBRE-EGZIABHER
University of Minnesota, Minneapolis, Minnesota

Received July 2003; Revised June 2004

ABSTRACT: *This research focuses on airborne integrity algorithms for shipboard relative GPS (SRGPS) navigation. Airborne autonomous detection is required for navigation threats that are undetectable by integrity monitors at a shipboard differential reference station. These threats can be separated into two basic categories: (1) aircraft receiver failures, and (2) signal-in-space anomalies whose effects depend on the displacement between the user and the ship. For the anticipated carrier-phase SRGPS navigation architecture, tracking-loop cycle slips are well-known threats in the first category. Ionospheric gradient and satellite orbit ephemeris anomalies are relevant threats of the second type. Airborne autonomous monitoring algorithms to detect these threats are described in this paper. Monitor performance is directly evaluated relative to the integrity requirements for aircraft shipboard landing navigation applications.*

INTRODUCTION

Shipboard-relative GPS (SRGPS) is an architectural variant of the Joint Precision Approach and Landing System (JPALS) that will provide high-accuracy and high-integrity differential GPS (DGPS) navigation for automatic shipboard landings. Unlike similar operations at ground-based airports, shipboard landing calls for higher navigation performance because of the mobility of the landing platform. The required vertical alert limit (VAL) for the navigation system is 1.1 m, with an associated integrity risk of approximately 10^{-7} [3]. It is desired that these integrity requirements be satisfied with a system availability of at least 99.7 percent for the nominal case when dual-frequency signals are available [6]. In the event of interference or jamming on one frequency, a target availability of 95 percent for single-frequency navigation is assumed. Because of the stringent nature of these specifications, carrier-phase DGPS (CDGPS) solutions are being pursued.

NAVIGATION: *Journal of The Institute of Navigation*
Vol. 51, No. 3, Fall 2004
Printed in the U.S.A.

Centimeter-level navigation performance is possible with CDGPS because carrier ranging measurement errors are normally very small (typically at the subcentimeter level). However, realization of this performance is dependent on the successful resolution of cycle ambiguities. The basic concept of CDGPS is that reference and user receive the signal from a given GPS satellite, and then the reference station broadcasts its measurement to the user. The user computes a single-difference phase by taking the difference between the user and reference carrier-phase measurements at time k for GPS satellite i. The mathematical expression of the single-difference carrier phase is

$$\Delta\phi_k^i = -\mathbf{e}_k^{i\,T}\mathbf{x}_k + \tau_k + \lambda N^i + v_k^i \qquad (1)$$

where $\mathbf{e}_k$ is the line-of-sight (unit) vector to satellite i, $\mathbf{x}_k$ is the displacement vector from the reference station to the user, λ is the wavelength of the carrier phase, N is the single-difference cycle ambiguity (integer), τ_k is the single-difference receiver clock bias, and v_k is the single-difference measurement error. When four or more satellites are in view, and the cycle ambiguities are known, the user position can be estimated with respect to the reference station with centimeter-level accuracy. Cycle

ambiguity resolution for the SRGPS application is discussed in [9, 11].

This paper focuses on the design of airborne integrity monitoring algorithms to detect and isolate navigation threats that are undetectable by integrity monitors at the shipboard differential reference station. (The development of shipboard integrity monitors is the subject of related concurrent work [4].) Such threats can be separated into two fundamental categories:

- Aircraft receiver failures
- Signal-in-space anomalies whose effects depend on the displacement between the user and the ship

For the CDGPS-based SRGPS navigation architecture, tracking-loop cycle slips are well-known threats falling into the first category. Relevant threats of the second class include ionospheric gradient and satellite orbit ephemeris anomalies. These latter threats may be detected by a ground-based reference facility having multiple reference antennas with long baselines. Ground-based ephemeris detection algorithms applicable to the Local Area Augmentation System (LAAS) are discussed in [15] and [16]. In contrast, SRGPS cannot detect such events at the shipboard reference station because it will be equipped with either a single reference antenna or multiple antennas with short baselines. In this paper, airborne autonomous algorithms designed to detect each of these threats are described. The performance of the proposed integrity monitors is directly evaluated relative to the navigation integrity requirements for shipboard landing of aircraft.

CYCLE SLIP DETECTION

The use of highly precise differential carrier-phase measurements in SRGPS enables the high navigation performance required for shipboard landing. However, this performance is dependent on maintaining continuous phase lock on the carrier signals. Interference, jamming, shadowing, and high dynamics may cause loss of phase lock and result in a sudden integer cycle jump in the carrier-phase observable. Such an event is known as a cycle slip, and integrity is compromised when it is not detected. Important prior cycle slip detection work was focused on the use of geometry-free linear combinations of available observables to test for abrupt discontinuities in the measurements. For example, in [12], the undifferenced geometry-free phase is used to detect cycle slips, whereas in [13] and [14], the double-difference widelane carrier-phase minus narrowlane pseudorange is used for this purpose. Both of these approaches require extensive filtering to detect cycle slips with high integrity.

In this section, the effectiveness of receiver autonomous integrity monitoring (RAIM) [5, 7, 8, 10] for cycle slip detection is explored. Single- and multiple-channel cycle slip threat models are considered for both single- and dual-frequency SRGPS architectures (using single-difference carrier-phase measurements). The traditional RAIM concept (see Appendix A) is extended in this research by applying integer and half-integer constraints on failure magnitude. In addition, the availability of the RAIM-based cycle slip detection function is directly evaluated in this work. Cycle ambiguity resolution is not strictly necessary for RAIM-based cycle slip detection because differences between sequential single-difference measurements can be used as the basis for detection.

SRGPS can potentially operate in two different modes: a nominal dual-frequency architecture and a single-frequency backup when interference or jamming exists in either the L1 or L2 band. Single- and multichannel cycle slips are considered for both the single- and dual-frequency architectures. The availabilities of RAIM function for cycle slip detection are evaluated independently for the single- and dual-frequency architectures.

Single-Frequency Architecture

For a single-frequency processing architecture (operating on either L1 or L2, in the event of jamming or interference on the other frequency), it is possible to detect single-channel cycle slips using carrier-phase RAIM. A symbolic illustration of such a scenario is presented in Figures 1a and 1b, which respectively show the nominal case of tracking six satellites in view and a cycle slip occurrence on Channel 6.

In RAIM fault detection, a missed detection is said to occur when the position error exceeds the required alert limit, but the least-squares residual is smaller than a predefined detection threshold. For SRGPS, the VAL is specified to be 1.1 m, and the detection threshold is defined to ensure a specified false alarm probability that is consistent with the continuity requirements for SRGPS. In this analysis, we assume a required false alarm probability of 10^{-7}.

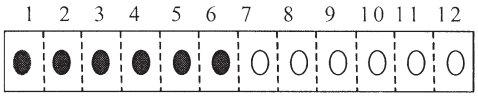

Fig. 1a–Normal Condition

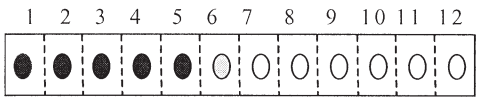

Fig. 1b–Cycle Slip Occurs on a Single Channel

To evaluate RAIM-based cycle slip detection performance, integer constraints on failure magnitude are applied. Specifically, it is assumed that the cycle slip occurs on the worst-case satellite channel with the worst-case bias of integer or half-integer magnitude.

Given a failure on a single satellite channel, the failure mode slope (FMS) for the satellite is defined as the ratio of the vertical position error to the magnitude of the residual vector. As illustrated in Figure 2, the normal measurement error dispersion (the ellipse shown in the figure) can be envisioned as sliding up and down along the FMS depending on the failure magnitude. In the figure, and in the remainder of this paper, $\|\mathbf{r}\|$ is the norm of the residual vector, and δx_3 is the vertical position error. Because there exist multiple satellite measurements, there are multiple FMSs. Therefore, we consider the limiting case in which the cycle slip occurs on the satellite channel with the steepest (worst-case) FMS.

The worst-case failure magnitude can be found by increasing the failure magnitude by half-cycle increments along the worst-case FMS. The probability of missed detection is computed at each increment, and the failure magnitude at which the probability of missed detection is maximized is selected as the worst-case cycle slip.

The probability of missed detection is defined as the joint probability that the position error is larger than the VAL and that the residual is smaller than the threshold. The mathematical representation of the probability of missed detection is provided in Appendix B. To ensure navigation integrity using RAIM, the probability of missed detection must be lower than the ratio of the allocated integrity risk requirement and the prior probability of the failure event. In this work, we typically assume a required missed detection probability of 10^{-4}, but this value is varied in the analysis to observe its influence on overall performance. Given a missed detection probability requirement, the performance of RAIM-based cycle slip detection is quantified by its service availability.

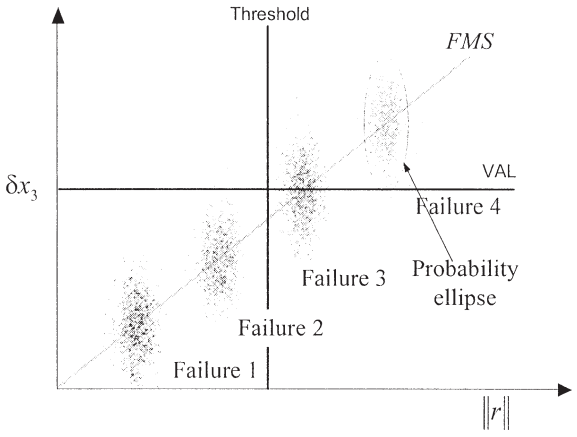

Fig. 2–Probability of Missed Detection Given Failure

Availability Analysis

Availability is defined as the fraction of time a navigation system is usable by the navigator. In the context of our RAIM analysis, a satellite geometry is declared unusable when the probability of missed detection of the worst-case cycle slip is larger than the prespecified minimum required to ensure integrity. RAIM availability is fundamentally limited by the "raw" availability of having at least five satellites in view. This raw availability is the maximum theoretical RAIM availability a user can achieve.

For the results to be meaningful, GPS satellite outages must also be considered in the computation of navigation service availability. In this analysis, the computed service availability is a weighted average of conditional availabilities using GPS constellation state probabilities as the weighting factors. The Minimum Standard constellation state probability model, defined in the GPS Standard Positioning Service Performance Specification [2], is used here.

Simulation Results

For a single-frequency processing architecture, the service availability of carrier-phase RAIM has been evaluated for the detection of full- and half-cycle slips on a single channel. Figures 3a, 3b, and 3c quantify the sensitivity of RAIM availability to ship location. The RAIM availability results were computed for three different ship longitudes—Indian Ocean (60° E), Atlantic Ocean (−60° E), and Pacific Ocean (−135° E)—and latitudes varying from 5° N to 45° N. Each figure shows results for a constant longitude and variable latitude assuming a 7.5 deg elevation mask, a single-difference measurement error standard deviation of 1 cm, and a required missed detection probability of 10^{-4}. In these figures, the bars represent, from left to right, the RAIM availability for detection of general failures with real-valued magnitude, cycle slips of integer or half-integer magnitude, cycle slips of integer magnitude, and the raw availability of having at least five satellites in view. The worst-case (lowest) service availability observed in these results occurs in Figure 3c (at 15° N, −135° E). It is clear, however, that even in this case, RAIM availability is higher than 97 percent, exceeding significantly the 95 percent target for single-frequency operation. It is also evident in the results that minimal availability improvement is derived from the application of integer or half-integer constraints on failure magnitude.

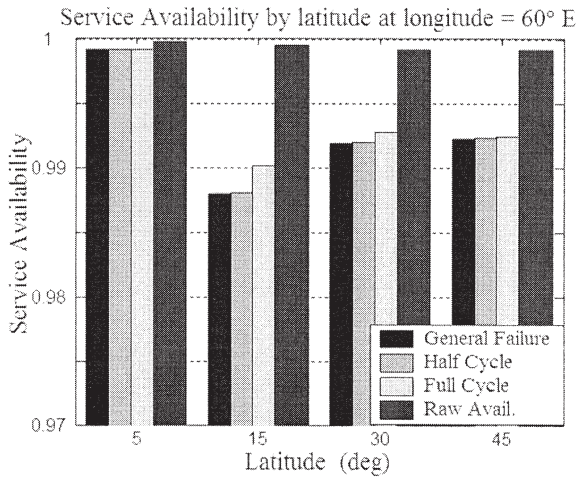

Fig. 3a–Service Availability at Longitude = 60° E

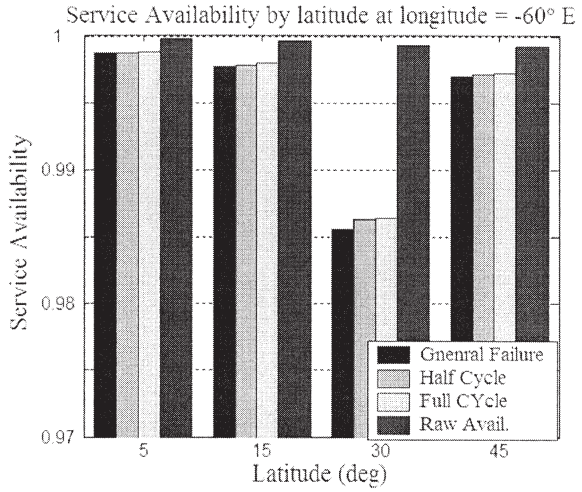

Fig. 3b–Service Availability at Longitude = −60° E

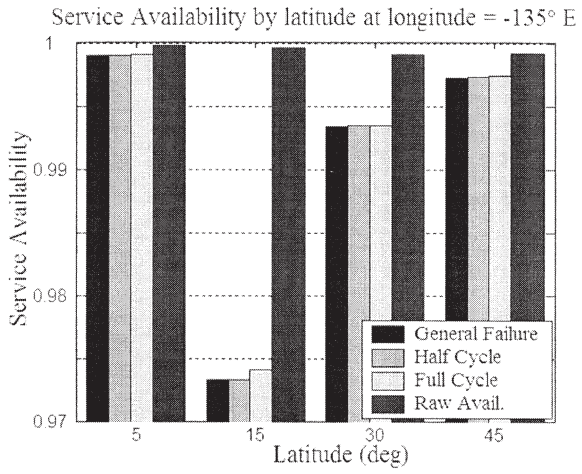

Fig. 3c–Service Availability at Longitude = −135° E

The sensitivity of RAIM availability to elevation mask is shown in Figure 4. The results in the figure were computed for the worst observed location found above, a required missed detection probability of 10^{-4}, and a single-difference measurement error standard deviation of 1 cm. The results show that RAIM availability is moderately sensitive to elevation mask, but that a 95 percent target for single-frequency operation is nevertheless easily achievable even for an elevation mask of 12.5 deg.

The sensitivity of RAIM availability to required missed detection probability is shown in Figure 5. The results in the figure were computed for the worst observed location defined above, an elevation mask of 7.5 deg, and a single-difference measurement error standard deviation of 1 cm. The results show that RAIM availability exhibits relatively weak sensitivity to required missed detection probability.

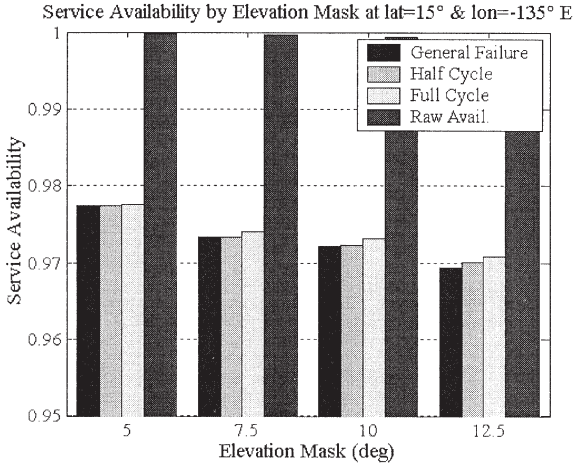

Fig. 4–Service Availability vs. Elevation Mask

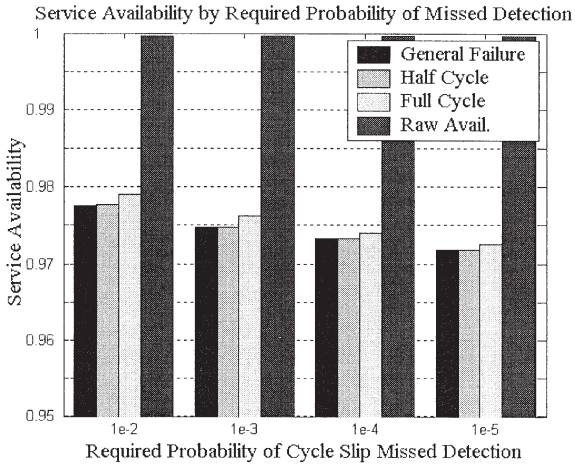

Fig. 5–Service Availability vs. Required Probability of Cycle Slip Missed Detection

Finally, Figure 6 quantifies the sensitivity of RAIM availability to carrier-phase measurement error standard deviation (σ). Again, the worst-case location, elevation mask of 7.5 deg, and required missed detection probability of 10^{-4} were used. Smaller nominal measurement error allows for tighter detection thresholds, thereby reducing the number of satellite geometries that have missed detection probabilities higher than 10^{-4}. As a result, RAIM availability is greater when measurement error standard deviation is lower. However, it is clear that service availability of greater than 95 percent is achievable for values of σ up to 1.8 cm.

Dual-Frequency Architecture

For a dual-frequency processing architecture (the nominal operating mode for SRGPS), greater measurement redundancy exists for the detection of cycle slips. Figures 7a and 7b show a symbolic illustration of simultaneous multichannel cycle slips in a dual-frequency system.

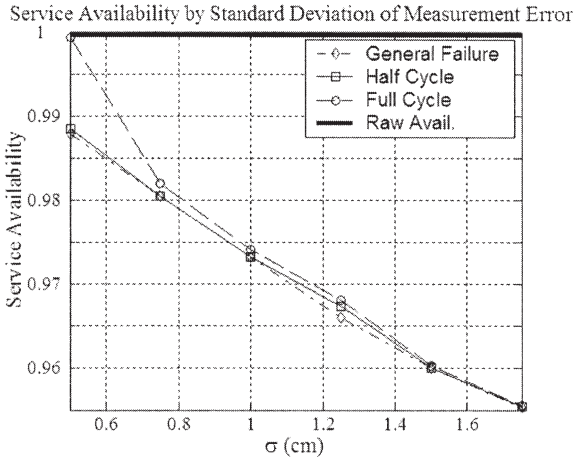

Fig. 6–Availability vs. Measurement Error

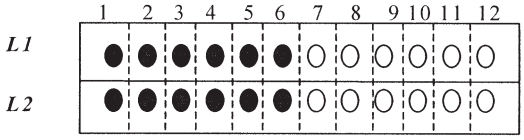

Fig. 7a–Normal Conditions

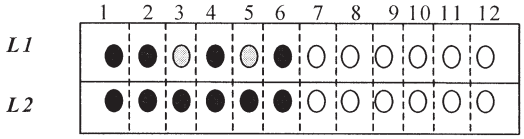

Fig. 7b–Cycle Slips Occur on L1 Channels 3 and 5

We first consider the case in which the cycle slips do not occur simultaneously on both frequencies for the same satellite. In this case, cycle slips can be detected by direct differencing of L1 and L2 single-difference ranging measurements:

$$\Delta\phi_{L12} = \phi_{L1} - \phi_{L2} = b + \Delta v \qquad (2)$$

where b is the bias due to the failure, and Δv is the nominal double-difference measurement error, which is distributed as $N(0,\sigma^2)$. Figure 8 illustrates a simple detection scenario in which a threshold T is set such that, under normal error conditions, the probability of false alarm is sufficiently low to ensure navigation continuity. Given a false alarm probability of 10^{-7} and double difference σ = 1 cm, a missed detection probability of 10^{-4} can be ensured only if the magnitude of the bias (b) is greater than 0.128 m. Because the magnitude of a full cycle slip on both L1 (19 cm) and L2 (24 cm) is always larger than the minimum detectable bias, the availability of the fault detection function using L1–L2 differencing is 100 percent for full cycle slips. In contrast, half-cycle slips (0.095 m for L1 and 0.12 m for L2) are smaller in magnitude than the minimum detectable bias for σ = 1 cm, and therefore cannot be detected with the specified missed detection probability. Such events can be detected with full availability only if the double difference $\sigma < 0.74$ cm.

Summary of Cycle Slip Detection

The availability performance of autonomous cycle slip detection using redundant GPS measurements is presented in Table 1. In summary, detection of cycle slips is guaranteed with the required availability for both single- and dual-frequency architectures provided that:

- For a single-frequency architecture, slips do not simultaneously occur on multiple channels.
- For a dual-frequency architecture, cycle slips are larger than one-half integer in magnitude and do not occur simultaneously for the same satellite on both frequencies.

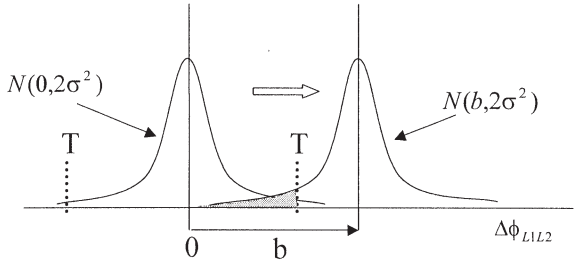

Fig. 8–Differencing Between L1 and L2

Table 1 — Summary of Cycle Slip Detection

	Single-Frequency Algorithm		Dual-Frequency Algorithm		
Required Service Availability	95%		99.7%		
				Multichannel	
Cycle Slip Occurrence	Single Channel	Multichannel	Single Channel	Same SV[a]	Different SVs
Half-Cycle Slip	Yes	No	No[b]	No	No[b]
Full Cycle Slip	Yes	No	Yes	No	Yes

[a]SV = satellite vehicle.
[b]RAIM is possible, but availability is lower than 99.7 percent.

To ensure comprehensive detection of such events, inertial augmentation of the integrity monitor will likely be required [1].

EPHEMERIS ANOMALY DETECTION

Each satellite broadcasts its own orbit ephemeris so users can compute the satellite location at any time of interest. Because the satellite locations are employed to calculate user position, an error in the satellite ephemeris will result in a navigation error. Under normal conditions, these errors are negligibly small for DGPS users. However, integrity considerations for aircraft precision landing navigation dictate that anomalous conditions must be quickly detected. Furthermore, orbit ephemeris anomalies cause navigation errors that are dependent on the time-varying displacement between the aircraft and reference receiver. Therefore, the impact of ephemeris anomalies on navigation must ultimately be assessed separately by each individual aircraft within the SRGPS service volume. In this context, carrier-phase RAIM is an attractive solution. The basis for observability of ephemeris failures using RAIM is that the magnitude of the residual test statistic will change proportionally during an approach as the distance between the aircraft and ship decreases. The effectiveness of such a "relative" RAIM method is therefore dependent on the magnitude of the observed change in the test statistic, which in turn is dependent on the total change in displacement during the approach within the SRGPS service radius.

Figure 9 illustrates the basic concept. The "service entry point" is the radius where the aircraft is first able to receive a reference measurement, and the "synthetic baseline" is the distance between the service entry point and aircraft location at any given time over the flight path. As the synthetic baseline increases, the ephemeris error will become detectable using relative RAIM. In this section, the autonomous ephemeris detection algorithm is described, and its effectiveness for SRGPS is evaluated.

Because SRGPS uses carrier-phase DGPS, navigation performance is dependent on the successful

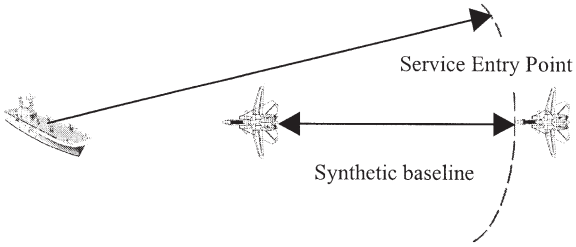

Fig. 9–Service Entry Point and Synthetic Baseline

resolution of cycle ambiguities corresponding to the GPS satellites in view. During measurement updates, the ephemeris error may affect the cycle ambiguity estimation process. In turn, incorrectly estimated cycle ambiguities can be used later during the approach to compute incorrect user (aircraft) position. To bound the position error caused by an ephemeris anomaly, we consider two limiting cases for cycle estimation implementations:

- *Limiting case 1* — Cycle ambiguities are established by averaging code against carrier.
- *Limiting case 2* — Cycle ambiguities are established using redundancy of carrier measurements.

Most implementations will use a hybrid of these two limiting scenarios.

Limiting Case 1

In this scenario, known as "geometry-free" cycle resolution, the ephemeris error does not affect the cycle ambiguity estimation process because time averaging the difference between code and carrier to measure the cycle ambiguity is not dependent on satellite geometry information. However, given that the cycle ambiguities are correctly estimated, errors will still be incurred during the positioning process because satellite geometry information is used. Specifically, positioning error due to satellite ephemeris error will be proportional to the displacement between the aircraft and reference receiver. In Figure 10, the solid line

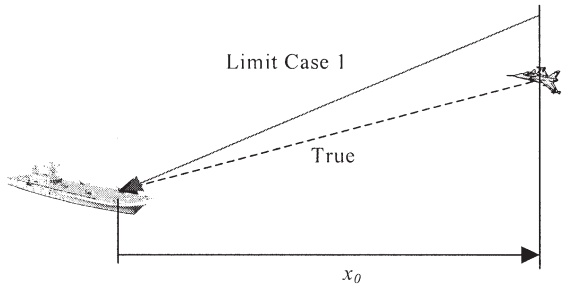

Fig. 10–Vertical Position Error Due to Orbit Ephemeris Error for Limiting Case 1

qualitatively illustrates the erroneous vertical position error history over the flight path. The mathematical expression for vertical position error is:

$$\delta x = \mathbf{H}^{+}_{3,i}\,\delta\mathbf{H}_i\mathbf{u}x \tag{3}$$

where **H** is the observation (geometry) matrix, $\mathbf{H}^+$ is its pseudoinverse, $\delta\mathbf{H}_i$ is the error in the observation matrix due to an ephemeris error on satellite i, **u** is the approach path direction (unit vector), x is the scalar displacement between the aircraft and reference antennas, and δx is the resulting vertical position error due to orbit ephemeris error.

The relative residual used for detection is

$$\delta\mathbf{r} \triangleq \mathbf{r}_0 - \mathbf{r} = (\mathbf{I} - \mathbf{H}\mathbf{H}^{+})\delta\mathbf{H}_i\,\mathbf{u}\alpha x \tag{4}$$

where $\mathbf{r_0}$ is the residual vector at the start (service entry) distance x_0, **r** is the residual vector at distance x, and the scalar factor α is defined as $(x_0 - x)/x$. Therefore, at a given distance x, the observable effect of the ephemeris on the residual is magnified by the value of α. In a RAIM interpretation, as illustrated in Figure 11, the FMS will decrease as α increases. We return to a discussion of the ramifications of the α parameter after developing limiting case 2.

Limiting Case 2

In this scenario, unlike limiting case 1, orbit ephemeris errors do have an effect on the cycle ambiguity estimation process. In this case, the floating cycle ambiguity estimates will absorb the effective ranging error induced by the ephemeris error. The resulting position error will be small near the effective cycle resolution distance (x_1) because the ephemeris error induced at this distance will be nearly cancelled by the error in the estimated cycle ambiguity. As the aircraft approaches the ship, however, the position error will increase proportionally with the displacement ($x_1 - x$) from the effective cycle resolution point. The maximum position error will occur at the aircraft touchdown point ($x = 0$), as shown in Figure 12. The mathematical expression for vertical position error in this case is

$$\delta x = \mathbf{H}^{+}_{3,i}\,\delta\mathbf{H}\mathbf{u}x^{*} \tag{5}$$

where $x^* = x_1 - x$, and x_1 is the equivalent cycle resolution distance.

The relative residual can be computed using equation (6), whose form is identical to equation (4). The difference between the two equations is simply that x has been replaced by x^*, and the scalar factor α in this case is defined to be $(x_0 - x)/x^*$:

$$\delta\mathbf{r} \triangleq \mathbf{r_0} - \mathbf{r} = (\mathbf{I} - \mathbf{H}\mathbf{H}^{+})\delta\mathbf{H}\mathbf{u}\alpha x^{*} \tag{6}$$

As illustrated qualitatively in Figure 13 for this limiting case, RAIM performance will improve as the distance $x_0 - x_1$ increases because the relative residual will grow larger before the first erroneous CDGPS position fix occurs (at $x = x_1$).

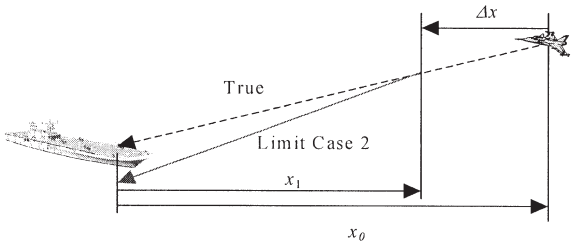

Fig. 12–Vertical Position Error Due to Orbit Ephemeris Error for Limiting Case 2

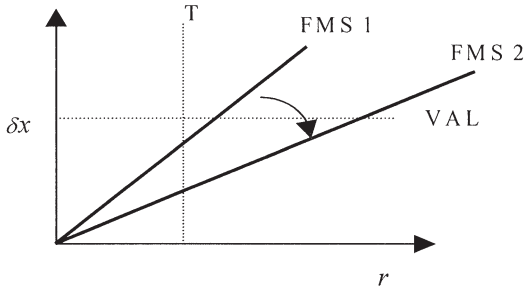

Fig. 11–Effect of Increasing α

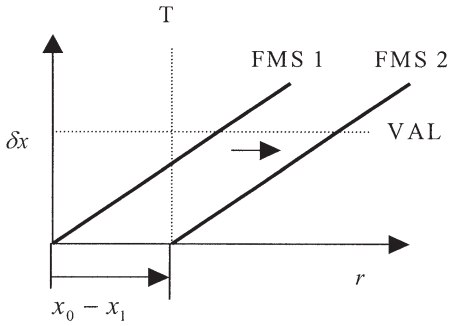

Fig. 13–Effect on RAIM of Increasing $x_0 - x_1$

Availability of Ephemeris Fault Detection

Because the mathematical structures of equation sets (3)/(4) and (5)/(6) are identical, it is advantageous to consider both cases simultaneously. In particular, we are interested in the value of α that will result in RAIM availability of 99.7 percent. Recall as α increases, the residual will be magnified relative to the position error for any given geometry; therefore, RAIM availability will be improved. In this regard, Figure 14 shows the RAIM availability results as a function of α. These results assume the worst-observed-case Central Pacific ship location defined earlier, a missed detection probability of 10^{-4}, single-difference σ = 1 cm, and three different elevation mask angles. The quantitative results clearly show that as α increases, availability is improved. When $\alpha = 5$, the 99.7 percent availability requirement is achieved. We therefore select the desired value $\alpha_{des} = 5$.

Although we want $\alpha \geq \alpha_{des}$ for each of the two limiting cases, the interpretation of this requirement is different for each. Using the definition of α for limiting case 1, it is required that x be smaller than $x_0/(1 + \alpha_{des})$ to ensure RAIM availability. (Conversely, for all distances in excess of $x_0/(1 + \alpha_{des})$, the RAIM function for ephemeris detection is not available with the desired missed detection performance.) Figure 15 shows, for several values of α, the maximum distance (x) within which RAIM is available as a function of the service entry distance (x_0). For example, given a service entry distance of 50 nmi, RAIM-based ephemeris detection is 99.7 percent available ($\alpha = 5$) within a radius of 8.33 nmi of the ship.

Using the definition of α for limiting case 2, it is required that x_1 (the effective cycle resolution distance) be smaller than x_0/α_{des} to ensure availability for all $x < x_1$. Figure 16 shows, for several values of α, the maximum effective cycle resolution distance (x_1) within which RAIM is available as a function of the service entry distance (x_0). For example, given a service entry distance of 50 nmi, RAIM-based ephemeris detection is 99.7 percent available ($\alpha = 5$) for $x < x_1$, if x_1 is 10 nmi or smaller.

Table 2 summarizes the necessary conditions imposed by the two limiting cases to achieve 99.7 percent availability ($\alpha = 5$) of the relative

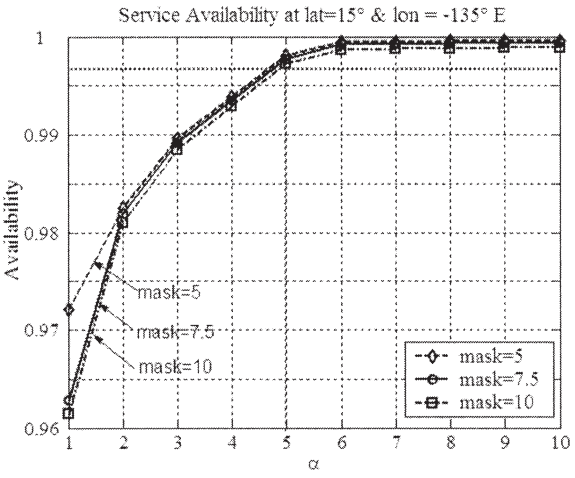

Fig. 14–Service Availability of Orbit Ephemeris Detection

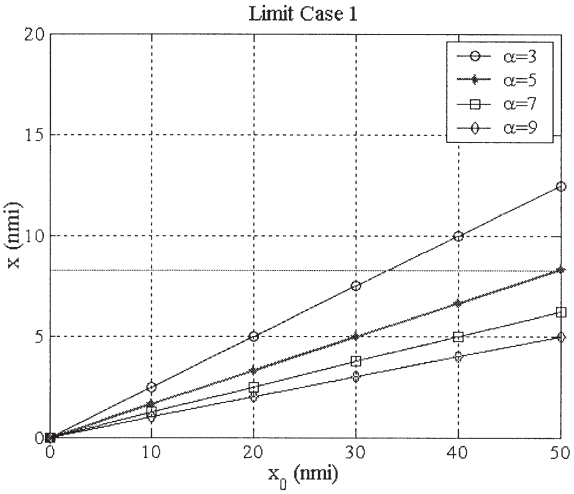

Fig. 15–x vs. x_0 for Limiting Case 1

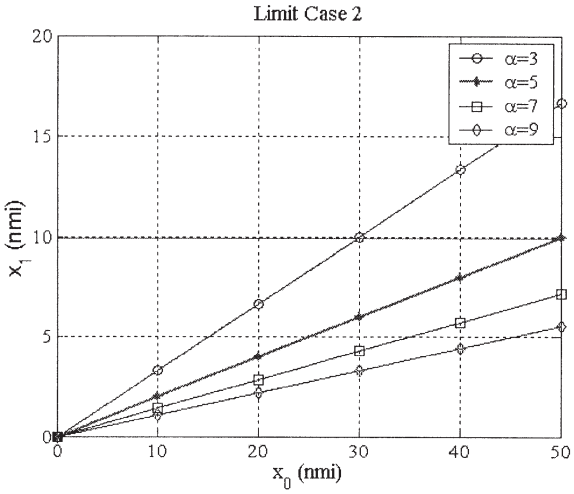

Fig. 16–x_1 vs. x_0 for Limiting Case 2

Table 2—Summary of Orbit Ephemeris Error Detection

Required Service Availability	99.7 percent => $\alpha = 5$	
Limiting Case	1	2
Necessary Condition	$x < x_0/6$	$x_1 < x_0/5$

RAIM ephemeris fault detection function. Both conditions should be satisfied to ensure RAIM performance for practical SRGPS navigation architectures.

IONOSPHERIC ERROR DETECTION

Nominally, the effects of ionospheric errors are mitigated by the use of DGPS. However, large ionospheric spatial gradients will cause differential ranging errors that are dependent on the displacement of the aircraft from the ship. Such sharp gradients are rare, being relatively more common near the auroral and equatorial regions, where the highest values of range delay are expected. Important prior work in ionospheric gradient detection has focused precisely on code–carrier divergence monitoring [17]. Here, we show that the relative RAIM algorithm discussed above can also be effective against anomalous ionospheric gradients affecting a given satellite. Unfortunately, in contrast with ephemeris failures, ionospheric gradient anomalies can potentially occur on multiple satellites simultaneously. (This is not the case for orbit errors since ephemeris data for each satellite are uploaded independently and at different times.) Nevertheless, because dual-frequency measurements will nominally be available with SRGPS, it is possible to use carrier-phase measurements to detect anomalous ionospheric gradients directly in real time during the aircraft approach. Moreover, the SRGPS user can also observe the anomalous ionospheric gradient with single-frequency measurements (for example, when interference or jamming is present on one frequency). This is true because of the divergence effect of the ionosphere on code and carrier measurements.

In this section, we consider an ionospheric threat model consisting of an anomalously large, constant spatial gradient during the approach. (More complex threat models, such as abrupt, nonlinear changes in ionospheric delay during approach, will be addressed in future work.) A means for autonomous detection of ionospheric spatial gradients is described, and the effectiveness of the detection algorithms is explicitly quantified.

Dual-Frequency Gradient Estimation

Assuming that a linear gradient model of the differential ionosphere is applicable for each satellite, the magnitude of the gradient can be directly observed using dual-frequency measurements taken over the aircraft approach. Taking the difference between L1 and L2 single-difference carrier-phase measurements when the aircraft is at a distance x from the reference station, we have, for a given satellite,

$$\Delta\phi_{L1} - \Delta\phi_{L2} = (1 - \gamma_{12})kx + \text{bias} + v \qquad (7)$$

where k is the differential L1 ionospheric gradient for the satellite, v is the nominal double-difference measurement error (assumed to be normally distributed with standard deviation σ_v), and γ_{12} is equal to $f_{L1}^2/f_{L2}^2 = 1.65$. We can estimate the gradient by applying equation (7) at the service entry distance x_0 and again at some distance x (where $x < x_0$) later during the approach, differencing the results, and dividing by $(\gamma_{12} - 1)(x_0 - x)$. The resulting ionospheric gradient estimate is distributed as

$$\hat{k} \sim N\left(k, \frac{\sigma_{\Delta I,\text{dual}}^2}{(x_0 - x)^2}\right) \qquad (8)$$

where $\sigma_{\Delta I,\text{dual}} = \dfrac{\sqrt{2}}{0.65}\sigma_v$.

Single-Frequency Gradient Estimation

The ionospheric gradient can also be directly (but less precisely) estimated using single-frequency measurements. Taking the difference between code and carrier single-difference measurements when the aircraft is at a distance x from the reference station, we have, for a given satellite,

$$\Delta\rho - \Delta\phi = 2kx + \text{bias} + v_{\rho-\phi} \qquad (9)$$

Following the above process, we estimate the gradient by applying equation (9) at the service entry distance x_0 and again some distance x later during the approach, difference the results, and divide by $2(x_0 - x)$. The resulting ionospheric gradient estimate is distributed as

$$\hat{k} \sim N\left(k, \frac{\sigma_{\Delta I,\rho-\phi}^2}{(x_0 - x)^2}\right) \qquad (10)$$

where $\sigma_{\Delta I,\rho-\phi} = \dfrac{\sqrt{2}}{2}\sigma_{\rho-\phi}$.

Effect of Ionospheric Gradient on Carrier-Phase Positioning

As was the case with ephemeris failures, the existence of an anomalous ionospheric gradient may affect the cycle ambiguity estimation process. In turn, incorrectly estimated cycle ambiguities can be used later during the approach to compute incorrect user (aircraft) position. To bound the position error caused by ionospheric gradient anomalies, we again consider the two limiting cases for cycle estimation already defined.

Let us assume that the effective cycle resolution distance is x_1, and the cycle resolution error due to the existence of the ionospheric gradient is δN. In this case, the effective single-difference carrier ranging error experienced at a distance x from the ship is

$$\delta\phi(x) = -\delta N - kx \qquad (11)$$

where nominal carrier-phase measurement errors are neglected for the moment. The error in the cycle ambiguity, δN, will differ for the two limiting-case cycle estimation scenarios. Table 3 shows the cycle ambiguity estimate errors along with the effective ranging error at $x = 0$ and $x = x_1$ computed from equation (11) for the two limiting cases. (Appendix C provides additional detail.) Figure 17 is an illustration of the corresponding position error histories. Because limiting case 1 results in worse position errors throughout the approach, only this case is considered in the analysis that follows.

Autonomous Ionospheric Gradient Detection Performance

Substituting the value of δN for limiting case 1 in Table 3 into the ranging error equation (11), it is possible to write an upper bound on vertical position error as

$$\delta x = \left\| \mathbf{H}^{+}_{3,:} \right\|_1 b\beta + v_x \tag{12}$$

where the following definitions are relevant:

- $\left\| \mathbf{H}^{+}_{3,:} \right\|_1$ is the 1-norm of $\mathbf{H}^{+}_{3,:}$
- $b \equiv \dfrac{k_{max}(x_0 - x)}{\sigma_{\Delta I}}$
- $\beta \equiv \dfrac{(2x_1 - x)}{x_0 - x}\,\sigma_{\Delta I}$ (13)
- $v_x \sim N(0, (\mathbf{H}^T\mathbf{H})^{-1}_{3,3}\sigma^2)$, and σ^2 is the single-difference measurement variance
- k_{max} is the maximum value of the ionospheric gradient for any satellite in view

Table 3—Cycle Resolution and Effective Ranging Measurement Errors

Limiting Case	δN	δφ(0)	δφ(x_1)
1	$-2kx_1$	$2kx_1$	kx_1
2	$-kx_1$	kx_1	0

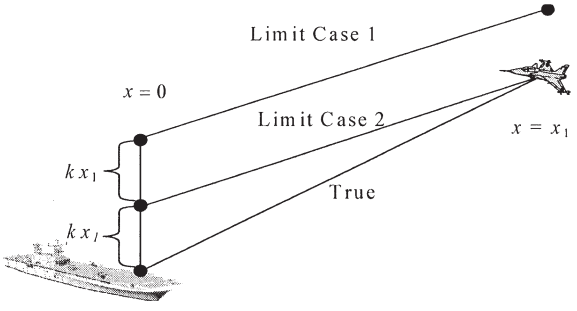

Fig. 17–Illustrated Position Error Histories Due to Ionospheric Gradient

The value of $\sigma_{\Delta I}$, defined just below equations (8) and (10), will depend on whether dual-frequency or single-frequency measurements are used to estimate ionospheric gradient. The normalized test statistic used for detection is

$$r \equiv \frac{\hat{k}_{max}(x_0 - x)}{\sigma_{\Delta I}} = b + \tilde{v}_k \tag{14}$$

where $\tilde{v}_k \sim N(0, 1)$.

As the ionospheric gradient (k_{max}) increases, b also increases, and both the position error (equation (12)) and the test statistic (equation (14)) become larger. In this case, we wish to find the value of β that will attenuate the effect of b on position error such that the availability of the detection function meets the target requirements. The detection function availability results are plotted as a function of β in Figure 18 for an elevation mask angle of 10 deg. It is evident that values of β smaller than or equal to 0.015 m for the nominal dual-frequency case and 0.0185 m for the single-frequency case will ensure sufficient detection function availability for the SRGPS application. We therefore define $\beta_{req} = 0.015$ and 0.0185 m for the dual- and single-frequency cases, respectively.

Given the definition of β in equation (13) and its required value (β_{req}) to ensure availability, we are able to define necessary conditions for cycle resolution distance as follows:

$$\frac{\beta_{req}}{\sigma_{\Delta I}} > 1: \quad \frac{x_1}{x_0} \le \frac{\beta_{req}/\sigma_{\Delta I}}{1 + \beta_{req}/\sigma_{\Delta I}} \tag{15}$$

$$\frac{\beta_{req}}{\sigma_{\Delta I}} < 1: \quad \frac{x_1}{x_0} \le \frac{\beta_{req}}{2\sigma_{\Delta I}} \tag{16}$$

These constraints are expressed graphically in Figure 19.

For example, given $\sigma_{\Delta I,dual} = 0.03$ m (for the nominal dual-frequency case) and $\sigma_{\Delta I,\rho-\phi} = 0.2$ m (for

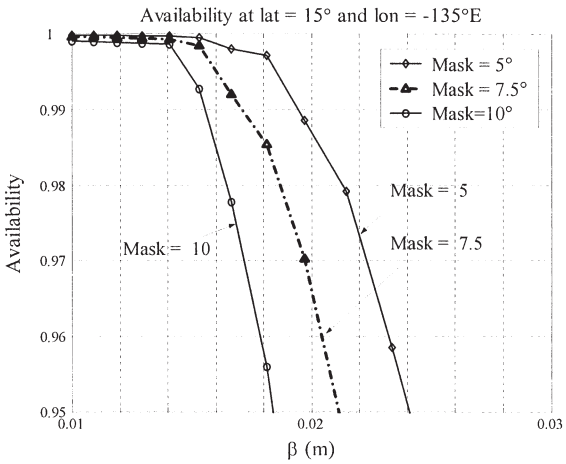

Fig. 18–Service Availability vs. β

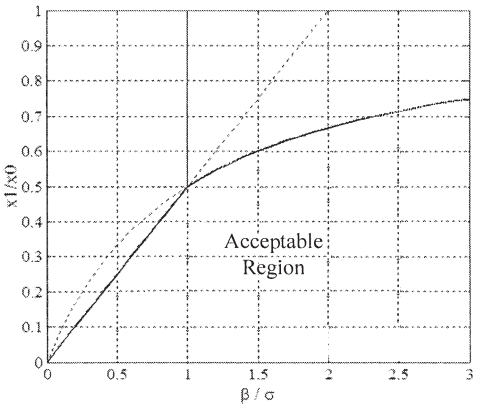

Fig. 19–Constraints on Cycle Resolution Distance

the single-frequency case), and also assuming a service entry distance (x_0) of 50 nmi, hazardous ionospheric gradients are detectable when the effective cycle resolution distance (x_1) is less than 2.3 nmi for the single-frequency case and 12.5 nmi for the dual-frequency case. The results for other values of x_0 are shown in Figure 20.

CONCLUSIONS

This research has focused on the design of SRGPS airborne integrity monitoring algorithms to detect and isolate navigation threats that are undetectable by integrity monitors at the shipboard differential reference station. Three specific navigation integrity threats have been addressed: airborne receiver cycle slips, orbit ephemeris anomalies, and ionospheric gradient anomalies.

A RAIM-based cycle slip detection algorithm has been developed and evaluated using integer and half-integer constraints on failure magnitude.

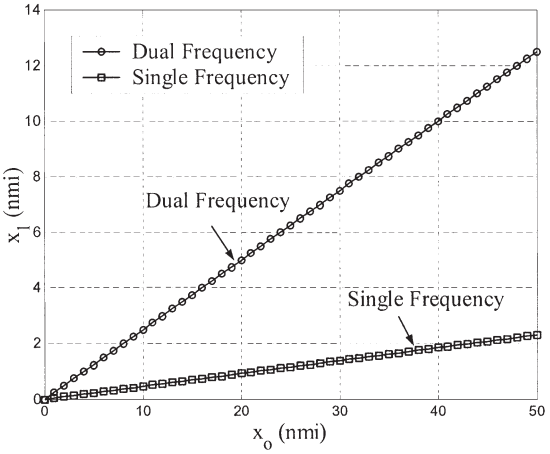

Fig. 20–Maximum Effective Cycle Resolution Distance Constraints

Based on the results, it has been determined that while RAIM can be effective for specific cycle slip threat models, the availability of the RAIM function is insufficient to protect against all classes of cycle slip threats. In this regard, it is recommended that the RAIM-based cycle slip detection function be augmented in future work with the integration of INS measurements.

A relative RAIM-based autonomous orbit ephemeris fault detection algorithm has also been developed, evaluated, and shown to be sufficient to provide protection against ephemeris threats. Necessary conditions for operational distance requirements have been specifically defined to ensure availability of the fault detection function.

Finally, autonomous ionospheric gradient detection algorithms have been designed using direct observation methods. Necessary conditions to ensure fault detection availability for both dual- and single-frequency implementations have been defined.

ACKNOWLEDGMENTS

The authors gratefully acknowledge the U.S. Navy (Naval Air Warfare Center) for supporting this research. However, the views expressed in this paper belong to the authors alone and do not necessarily represent the position of any other organization or person.

Based on a paper presented at The Institute of Navigation's National Technical Meeting, Anaheim, California, January 2003.

APPENDIX A: BASIC RAIM CONCEPTS

Consider the generalized linear observation equation

$$\mathbf{z} = (\mathbf{H} - \delta\mathbf{H})\mathbf{x} + \mathbf{v} \qquad \text{(A-1)}$$

where $\mathbf{H}$ is the observation matrix, $\mathbf{z}$ is the measurement vector; $\mathbf{x}$ is the vector to be estimated; and $\mathbf{v}$ and $\delta\mathbf{H}$ are the unknown errors in the measurement vector and observation matrix, respectively.

The least-squares solution to equation (A-1) is

$$\hat{\mathbf{x}} = \mathbf{H}^{+}\mathbf{z} \qquad \text{(A-2)}$$

where $\hat{\mathbf{x}}$ is the estimated vector, and $\mathbf{H}^{+} \equiv (\mathbf{H}^{T}\mathbf{H})^{-1}\,\mathbf{H}^{T}$. The corresponding least-squares estimate error under normal conditions is defined as

$$\delta\mathbf{x} \equiv \hat{\mathbf{x}} - \mathbf{x} \qquad \text{(A-3)}$$

The least-squares residual vector $\mathbf{r}$ is a measure of the consistency of the measurement vector $\mathbf{z}$ subject to the observation matrix $\mathbf{H}$, and is expressed simply as

$$\mathbf{r} \equiv \mathbf{z} - \mathbf{H}\hat{\mathbf{x}} \qquad \text{(A-4)}$$

Combining equations (A-1), (A-2), and (A-4), the residual vector can be expressed in terms of the measurement and observation matrix errors:

$$\mathbf{r} = (\mathbf{I} - \mathbf{H}\mathbf{H}^{+})(\delta\mathbf{z} - \delta\mathbf{H}\mathbf{x}) \tag{A-5}$$

where, under normal error conditions,

$$\delta\mathbf{H} \cong 0 \text{ and } \mathbf{v} \sim N(0,\sigma_z^2\mathbf{I}_n) \tag{A-6}$$

The simplest form of RAIM fault detection is based on the use of the magnitude of the residual vector $\|\mathbf{r}\|$ as a statistical indicator of possible navigation failure. Under normal error conditions, the test statistic is distributed as

$$\frac{\|\mathbf{r}\|^2}{\sigma_z^2} \sim \chi^2(n - m) \tag{A-7}$$

where n is the number of measurements, m is the number of unknowns, and χ^2 (n − m) is the chi-square distribution with (n − m) degrees of freedom.

APPENDIX B: COMPUTATION OF MISSED DETECTION PROBABILITY

Consider a failure of magnitude b on channel i. The vertical position error i can then be expressed as

$$\delta x = \mathbf{H}_{3,i}^{+}b + \mathbf{H}_{3,:}^{+}v \tag{B-1}$$

where $\mathbf{H}_{3,:}^{+}$ is the third row of the pseudo-inverse (i.e., the row corresponding to the vertical position state) of the observation matrix **H**.

Using equation (B-1), the probability that the position error is larger than the VAL can be expressed mathematically as

$$\begin{aligned} P\left(|\delta\mathbf{x}_3| > VAL\,|b\right) &= P(\mathbf{H}_{3,:}^{+}v > VAL - \mathbf{H}_{3,i}^{+}b) \\ &\quad + P(\mathbf{H}_{3,:}^{+}v > -VAL - \mathbf{H}_{3,i}^{+}b) \end{aligned} \tag{B-2}$$

where the terms on the right-hand side of equation (B-2) represent the tail probabilities of a normal distribution.

Because the n × 1 vector **r** is orthogonal to the columns of the n × 4 observation matrix **H**, the elements of **r** are not all independent. Therefore, it is enough to consider the (n − 4) space orthogonal to the columns of **H**. This is called parity space, and details of the parity space method are explained in [8, 10].

Given a bias failure of magnitude b on channel i, the (n − 4) × 1 parity vector **p** can be expressed as

$$\mathbf{p} \sim N(\mathbf{C}_{:,i}b,\sigma_v^2\mathbf{I}_{n-m}) \tag{B-3}$$

where **C** is the left null space of **H**. It is shown in [5] that

$$p\left(\|\mathbf{r}\| < T\,|b\right) \cong P\left(v > \|\mathbf{C}_{:,i}\|_2 b - T\right) \tag{B-4}$$

where $\mathbf{P}\left(v > \|\mathbf{C}_{:,i}\|_2 b - T\right)$ represents the tail probability of a normal distribution.

Finally, the joint probability of missed detection given a failure b can be expressed simply as

$$\begin{aligned} P\left(MD\,|b\right) &= P\left(\delta\mathbf{x}_3 > VAL, \|\mathbf{r}\| < T\,|b\right) \\ &= [P(\mathbf{H}_{3,:}^{+}v > VAL - \mathbf{H}_{3,i}^{+}b) + P(\mathbf{H}_{3,:}^{+}v > \\ &\quad -VAL - \mathbf{H}_{3,i}^{+}b)]P\left(v > \|\mathbf{C}_{:,i}\|_2 b - T\right) \end{aligned} \tag{B-5}$$

where v is distributed as in equation (A-6). For any given failure magnitude b, the right-hand side of equation (B-5) is easy to evaluate.

APPENDIX C: RANGE MEASUREMENT ERROR DUE TO IONOSPHERIC GRADIENT

The observation equation for carrier positioning can be expressed as

$$\phi(x) = \mathbf{e}^{\mathbf{T}}\mathbf{x} + N - I(x)$$

Given an estimate of the cycle ambiguity

$$\hat{N} = N + \delta N$$

and the adjusted carrier-phase observable is

$$\phi(x) - \hat{N} = \mathbf{e}^{\mathbf{T}}\mathbf{x} + \delta\phi(x) \tag{C-1}$$

where

$$\delta\phi(x) = -\delta N - I(x) \tag{C-2}$$

δN is the error in the cycle ambiguity, and nominal carrier-phase measurement errors are neglected for the moment.

Let us assume that the cycle is resolved at distance x_1. The limiting case effective cycle ambiguity errors are:

- Limiting case 1—$\delta N = \delta\phi - \delta\rho = -2I(x_1)$
- Limiting case 2—$\delta N = -I(x_1)$ (C-3)

where $I(x_1)$ is the differential ionospheric delay at the distance x_1. Expressed in terms of the differential ionospheric gradient k:

$$I(x_1) = kx_1 \tag{C-4}$$

Finally, substituting equations (C-3) and (C-4) into equation (C-2), the limiting case effective range measurement errors due to the ionospheric gradient in Table 3 can be computed.

REFERENCES

1. Altmayer, C., *Cycle Slip Detection and Correction by Means of Integrated Systems*, Proceedings of The Institute of Navigation's National Technical Meeting, Anaheim, CA, January 2000.
2. *Global Positioning System Standard Positioning Service Signal Specification*, 2nd Edition, Proceedings of The Institute of Navigation's Annual Meeting, June 1995.
3. JPALS Test Planning Working Group, *Architecture and Requirements Definition: Test and Evaluation Master Plans for JPALS*, Proceedings of The Institute

of Navigation's National Technical Meeting, January 19, 1999.
4. Koenig, M., D. Gebre-Egziabher, S. Pullen, U. S. Kim, B. Pervan, and F. C. Chan, *Analysis of Reference Antenna Motion on the JPALS Shipboard Integrity Monitor*, Proceedings of The Institute of Navigation's National Technical Meeting, Anaheim, CA, January 2002.
5. Lee, Y., *New Techniques Relating Fault Detection and Exclusion Performance to GPS Primary Means Integrity Requirements*, Proceedings of The Institute of Navigation's ION GPS-95, Palm Springs, CA, September 1995.
6. *Operational Requirements Document (ORD) for Joint Precision Approach and Landing System (JPALS)*, USAF 002-94-I.
7. Parkinson, B. W. and P. Axelard, *Autonomous GPS Integrity Monitoring Using the Pseudorange Residual*, NAVIGATION, Journal of The Institute of Navigation, Vol. 35, No. 2, 1988, pp. 255–74.
8. Pervan, B. and B. W. Parkinson, *Autonomous Fault Detection and Removal Using GPS Carrier Phase*, IEEE Transactions on Aerospace and Electronic Systems, Vol. 34, No. 3, July 1998.
9. Pervan, B. and F. C. Chan, *System Concepts for Cycle Ambiguity Resolution and Verification for Aircraft Carrier Landings*, Proceedings of The Institute of Navigation's ION GPS-2001, Salt Lake City, UT, September 2001.
10. Sturza, M. A., *Navigation System Integrity Monitoring Using Redundant Measurements*, NAVIGATION, Journal of The Institute of Navigation, Vol. 35, No. 4, 1998–1989.
11. Heo, M. B., B. Pervan, S. Pullen, J. Gautier, P. Enge, and D. Gebre-Egziabher, *Robust Airborne Navigation Algorithms for SRGPS*, Proceedings of the IEEE Position, Location, and Navigation Symposium (PLANS 2004), Monterey, CA, April 2004.
12. Blewitt G., *An Automatic Editing Algorithm for GPS Data*, Geophysical Research Letters, Vol. 13, No. 4, pp. 199–202.
13. Gao, Y. and Z. Li, *Cycle Slip Detection and Ambiguity Resolution Algorithms for Dual-Frequency GPS Data*, Marine Geodesy, Vol. 22, No. 4, pp. 169–81.
14. Bisnath, S. B., *Efficient, Automated Cycle Slip Correction of Dual-Frequency Kinematic GPS Data*, Proceedings of The Institute of Navigation's ION GPS-2000, Salt Lake City, UT, September 2000.
15. Pervan, B. and F. C. Chang, *Detecting Global Positioning Satellite Orbit Errors Using Short-Baseline Carrier-Phase Measurements*, Journal of Guidance, Control, and Dynamics, Vol. 26, No. 1, January–February 2003.
16. Gratton, L., B. Pervan, and S. Pullen, *Orbit Ephemeris Monitors for Category I LAAS*, Proceedings of the IEEE Position, Location, and Navigation Symposium (PLANS 2004), Monterey, CA, April 2004.
17. Luo, M., S. Pullen, D. Akos, G. Xie, S. Datta-Barua, T. Walter, and P. Enge, *Assessment of Ionospheric Impact on LAAS Using WAAS Supertruth Data*, Proceedings of The Institute of Navigation's Annual Meeting, Albuquerque, NM, June 2002.